December 2019

The Effect of Geometric Defects and Porosity on the Mechanical Behavior of Additively Manufactured SS 316L and AlSi10Mg Components

Benjamin A. Smith
Clemson University, bas2@g.clemson.edu

THE EFFECT OF GEOMETRIC DEFECTS AND POROSITY ON THE
MECHANICAL BEHAVIOR OF ADDITIVELY MANUFACTURED
SS 316L AND ALSI10MG COMPONENTS

A Thesis
Presented to
the Graduate School of
Clemson University

In Partial Fulfillment
of the Requirements for the Degree
Master of Science
Mechanical Engineering

by
Benjamin Aaron Smith
December 2019

Accepted by:
Garrett Pataky, Committee Chair
Huijuan Zhao
Xin Zhao

ABSTRACT

Additive manufacturing (AM) is becoming increasingly popular in the automotive, aerospace, energy and healthcare industries. Standards for critical defect sizes and porosity levels in AM materials have not been established. A critical porosity manufactured defect relationship which can qualify components for safe use needs to be developed. Defects including a quarter crack, an internal void, and a through-hole were intentionally manufactured into SS 316L and AlSi10Mg AM tubular tensile specimens to investigate and improve the understanding of the ductility-defect-porosity relationship of AM Metals. SS 316L and AlSi10Mg compression specimens were tested from different build heights and locations on the build plate to explore the effects of spatial location on the material properties. Thin single edge notch tensile fracture toughness specimens with AM notch and diamond saw notch were studied to investigate the apparent fracture toughness of thin AM specimens. Levels of porosity were introduced by reduced laser power in all the AlSi10Mg specimens. This study helps define the relationship between defects, porosity, and ductility of AM SS 316L and AlSi10Mg and compares this relationship to conventional metals. From the results of this study, AM SS 316L and AM AlSi10Mg follow conventional knowledge about stress concentration and ductility for metals.

There was no significant difference in fracture toughness between the AM and diamond saw notch in the fracture toughness specimens. The SS 316L compression specimens closer to the build plate had increased material properties while the AlSi10Mg compression specimens had similar material properties throughout. The material properties of the SS 316L and AlSi10Mg compression specimens varied by the build plate location.

Geometric defects decreased the ductility and strength for all the tubular tensile specimens. With a significant increase in porosity, the mechanical behavior started to be dominated by the porosity over the intentionally manufactured geometric defects. The mechanical behavior of the ductile SS 316L tubular specimens was driven by the reduction in the cross-sectional area while the more brittle AlSi10Mg was driven by stress concentrations. From this study, AM SS 316L and AlSi10Mg produced by selective laser melting had similar mechanical behavior to traditional ductile and brittle metals.

ACKNOWLEDGMENTS

TABLE OF CONTENTS

LIST OF FIGURES

LIST OF TABLES

1. Chapter 1: Introduction

1.1 Motivation

Additive manufacturing (AM) is becoming increasingly popular in industries such as automotive, medical, energy, and aerospace, because of the flexibility and customization over traditional manufacturing methods [1,2]. For the past five years, there has been a 40% growth in the sale of AM powdered metal alloys [3]. ASTM has developed standards for describing AM in terms of geometry, tolerances, and nomenclature, but there is not a defined standard for critical defect sizes and porosity level for any AM material in terms of quality control [4–7]. A critical defect-porosity relationship needs to be determined to qualify AM metal components for safe use.

Understanding how the build height and location affect the material properties is also important for characterizing AM material for safe use. The effects of the build plate height and location have been studied, but the observations and conclusions vary for each study and material [8–10]. In a study on AM SS 304, results concluded components closer to the build plate height had finer grain size and increased mechanical properties [10]. In another study on AM Inconel 718 components, the build height had no significant effect on the material properties[9]. This thesis investigates the effect of build plate height and location for SS 316L and AlSi10Mg.

When making components it is essential that the material properties meet a certain standard for design. Knowing the fracture toughness for thin complex AM structural

components is critical for designing against catastrophic failure. As the thickness decreases the apparent fracture, toughness generally increases and above a certain thickness, the apparent fracture toughness is constant [11]. The effect of porosity on the fracture toughness of AM parts can provide additional information on the influence of porosity on the mechanical behavior for AM metals. The diamond saw and AM notches were studied to compare the effects of the manufacturing method to produce the notch.

Defects will be present in AM components and it is important to be able to qualify the size and shape of defects for safe-use. The function and safety of components could be put at risk if the mechanical properties are lower than required. A critical porosity manufactured defect relationship which can qualify components for safe use needs to be developed. Once this porosity manufactured defect relationship is established, methods such as computed tomography (CT) and acoustic resonance testing can be used to identified components safe for use [12,13]. The goal of this thesis project is to move the field closer to an understanding of this material-defect-porosity relationship.

1.2 Research Questions

Additive manufacturing has become increasingly popular in commercial applications. Defects will always occur with AM and will be a concern for qualify components for safe-use. The focus of the thesis is expanding the understanding of the ductility-defect-porosity relationship in AM metals.

1. What is the relationship between porosity, geometric defects and ductility for AM metals?

2. What level of the ductility-defect-porosity relationship understanding is needed to qualify AM components for safe use?

3. What knowledge about stress concentrations and ductility for conventional metals can also be applied to AM metals?

4. How does porosity and type of notch affect the fracture toughness of single edge notch AlSi10Mg and SS 316L fracture toughness specimens?

5. How does spatial location (height, build plate location) affect the material properties of AM SS 316L and AM AlSi10Mg in compression?

1.3 Background

Additive manufacturing is fundamentally different from traditional, subtractive manufacturing methods, as the material is added layer by layer to build the component. Complex geometries and custom components are possible with AM that would have been cost-prohibitive or impossible with traditional manufacturing methods. AM can produce a near-net shape compared to traditional manufacturing methods that might use multiple machines and tooling [1]. Using AM can drastically reduce the tooling cost and lead time to make low production and custom component [1,14]. There is a variety of AM process and they each have unique benefits and advantages.

Most metal AM processes fall into three categories: powder bed systems, powder feed systems, and wire feed systems [15,16]. In a powder bed system, metal powder is spread out over the bed and a laser melts the powder layer by layer [15–17]. In a powder feed system, metal powder is fed throw a nozzle, and the powder is melted by a laser on to the component and built layer by layer [15,16]. In a wire feed system, the metal wire is fed

into the laser beam or energy source to metal the wire and the component is built up layer by layer [16].

One type of powder bed metal AM, and the process used in this study is selective laser melting (SLM). SLM is a popular AM method for producing aluminum and stainless steel alloys [18] [19]. SLM is a powder bed additive manufacturing process that uses a high-intensity laser to melt powder metal together layer by layer to build a component [17,20,21]. This study focused on ductile SS 316L, moderate-ductility heat-treated AlSi10Mg, and brittle as-built AlSi10Mg tubular tensile specimen produced with SLM to compare the material behavior of ductile and brittle AM materials with intentionally manufactured defects

Geometric defects can occur internally in AM materials because of the layer by layer manufacturing process. Some common defects in AM components include gas bubbles, voids from lack of fusion, keyhole porosity, surface skin defects such as roughness and cracks, and layer separation [22,23]. Voids are individual defects formed throughout the AM material and reduce the density and can lead to premature failure. Porosity is a term for the decrease in the overall relative density of the material from the formation of voids which comes either lack of fusion induced, gas-induced or keyhole induced [23]. Porosity can be powder-induced, process-induced, or an artifact of solidification [20]. To complicate the matter, there are multiple variables at play during the building process creating a complex process-property relationship that must be optimized for the specific material and individual build. Studies on optimizing the processing parameters, including laser power, scan speed, and hatch distance, have shown a decrease in overall porosity and

material variability [24–26]. Layer separation or delamination is the separation of adjacent layers, because of incomplete melting between layers [20]. Cracking can occur in AM from unmelted particles between layers. Thermal gradients can also cause cracks to form [22]. Nevertheless, because of the complexity in optimizing parameters, it is expected that internal porosity in these materials will continue to be a present feature well into the evolution of this technology.

Voids can be caused by a combination of different build parameters, and there are three types of mechanisms that have been identified by which void defects are produced [23]. First, at very high power density, deposition, or melting, AM may be performed in keyhole mode. With poor control, the keyhole can be unstable, collapse, and entrap vapor. If the applied power, scan speed, and beam size are above a certain value, spatter injection may occur in a process called keyhole formation [20]. In keyhole formation, the power density is high enough to cause evaporation of the metal and the formation of plasma. Metal evaporation causes the development of a vapor cavity. The collapse of the cavity can leave a void in the wake of the laser beam [27]. Second, gas can be entrapped inside the powder particles during the powder atomization process. The entrapped gas cause gas pores. Gas pores may also be caused by the entrapment of shielding gas or alloy vapors inside the melt pool. Third, lack of fusion defects can be caused by inadequate penetration of the molten pool into either the substrate or into the previous layer [23]. When there is not enough laser power to melt the powder lack of fusion can occur which results in porosity and unmelted particles. Lack of fusion regions may be identifiable by un-melted powder particles in or

near the pore [20]. Each of these types of voids can be caused by incorrect laser power and contamination in the material.

AM can be used with numerous powder metals alloys including stainless steel, aluminum alloys, and titanium alloys [25,28]. It is critical to know how each type of defect affects different materials. Typically, brittle metals are generally more sensitive to stress concentrations and have rapid crack propagation compared to ductile metals [11]. The effects of defects on powder metal AM materials may not be consistent across all AM metals and may not align with ductile and brittle wrought metals. It is important to understand how defects affect the material behavior of AM materials. Identifying the critical defect size and type of defect is vital for quality control and reliability prediction of AM components. By knowing the critical defect type and size for each AM material, techniques can be taken to inspect for these defects. Geometric defects in AM can be stress concentrations that could be an initial site for crack growth and lead to failure.

In this study, AM metal specimens were studied to investigate the ductility-defect-porosity relationship, the effect of spatial location on the build plate, and fracture toughness of thin AM specimen. Geometric defects (internal voids, through-holes, and quarter cracks) were intentionally manufactured in AlSi10Mg and SS316L tubular tensile specimens using SLM to observe the effect of porosity, geometric defects, and ductility on the mechanical behavior. Fracture toughness specimens were studied to evaluate effective fracture toughness on thin AM specimens with AM notches and diamond saw notches at different porosity levels. Compression specimens were studied to observe the impact the distance from the build plate and location on the build had on the material properties. There

have been studies on the effect of build plate location on the material properties of powder bed AM materials [29]. Smaller grain sizes have been observed closer to the build plate, resulting in better material properties compared to further away from the build plate for SS 304 [30,31].

The two materials, SS 316L and AlSi10Mg, were chosen based on their expected mechanical behavior ranging from relatively brittle in the case of the aluminum material to relatively ductile in the case of the stainless steel. Furthermore, the effect of relative material porosity induced from laser power levels was varied at three levels in the AlSi10Mg specimens. It is known that bulk porosity will also affect the overall ductility of a material [32,33], yet it is unclear how the geometry of a key defect will interact will the bulk porosity. This study helps define the relationship between defects, porosity, and ductility of AM SS316L and AlSi10Mg and compares this relationship to conventional metals.

2. Chapter 2: Materials

2.1 Materials and Characterization

AM SS 316L and AM AlSi10Mg were the two materials studied to represent a ductile material and a brittle material. SS 316L and AlSi10Mg are two common metals used for direct metal laser sintering (DMLS) [34]. The SS 316L specimens were produced on a single build plate in a Renshaw AM 400 operating at a nominal laser power of 200W and a hatch distance of 0.06 mm. Three different build plates of AlSi10Mg were produced

on an EOS M290 with a laser speed of 1300 mm/s and a hatch distance of 0.19 mm, each with a different laser power output.

AlSi10Mg build plates A, B, and C were manufactured at different laser power levels. Build plate A was at 370 W; the recommended operating parameter from the manufacturer. Build plate B and build plate C reduced the laser power to 227.5W (75% reduction) and 185W (50% reduction) of the first build, respectively. The goal of reducing laser output was to observe the effect this would have on the overall porosity; and thus, criticality of additional intentionally introduced geometric flaws. The relative change in laser power induced porosity can be seen in the fracture surface of dog bone specimens in Figure 1. The relative density in Table 1 was calculated using the Archimedes method with water and a basket support arrangement to follow ASTM standard B311[35]. The density measurement of each build plate was an average of four square column specimens that were printed beside the tubular tensile specimens. The middle section of the compression specimen which had a similar height to the defect in the tubular tensile specimens was used for the density measurements. The density of 2.67 g/cm^3 was used for the fully dense AlSi10Mg in the calculation for the relative density [36], while the SS316L assumed a full density of 7.99 g/cm^3 [37]. The density measurement for build plate C was outside the two percent porosity as defined in the ASTM standard B311 [35].

It is common to heat treat AlSi10Mg to increase ductility with a trade-off of strength [36,38]. As a worst-case scenario of limited ductility, some engineered tubular specimens were not heat-treated in the present study. The remaining tubular AlSi10Mg specimens were heat-treated to provide a material that was used in real-world applications

and had a ductility between SS 316L and the as-built AlSi10Mg. Heat treatment was performed on a series of characterization coupons on the build plates to obtain baseline material properties between the heat-treated and as-received states. The heat treatment followed a common stress-relief annealing process of placing the samples at 300°C for 2 hours followed with a static air quench [39,40].
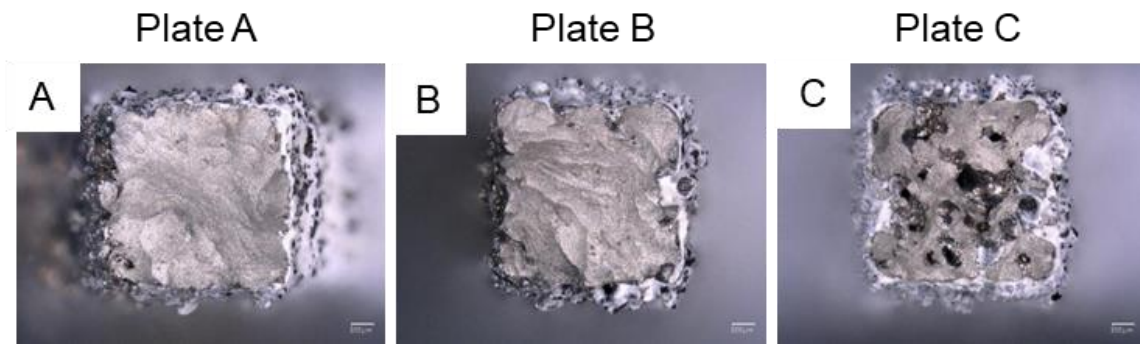
Figure 1: Images of the fracture surface of dog bone specimens from AlSi10Mg build plate A, build plate B, and build plate C show the different levels of porosity (dark spots) and build quality.

Table 1: Average relative density measurement (ASTM B311) of AlSi10Mg with build plate A laser power (370W), build plate B laser power (277.5W) and build plate C laser power (185W) as well as the 316 L comparator build.

Specimen	Average Relative Density
Build Plate A AlSi10Mg	99.5 %
Build Plate B AlSi10Mg	99.3%
Build Plate C AlSi10Mg	94.9 %
316L Stainless Steel	99.2%

Baseline mechanical testing was also performed by Sandia National Laboratories on a variety of coupons from the build plates to fully characterize the mechanical behavior before testing the engineered tubular specimens with intentional geometric defects.

Samples had a nominal gauge cross-section of 6.25 x 6.25 mm^2 and a gauge length of 32.5 mm [39]. Samples were tested in the as-printed condition except for a few heat-treated AlSi10Mg samples from both build plates for comparators. Monotonic tensile tests were performed until failure at strain rates of 10^{-3} mm/mm/s and used a virtual extensometer via digital image correlation (DIC) to obtain strain and a load cell to obtain force. The results of these tests can be found in Table 2. The SS 316L material shows the highest strength and ductility, as expected. The AlSi10Mg was both affected by thermal processing history and laser power. The significant increase in lack of fusion porosity with build plate C had a detrimental effect on the mechanical properties; the build plate C displayed a 6.5% lower yield strength, 31.2% lower ultimate tensile strength, and 67.8% lower ductility compared to build plate A for the as-received case. Similar trends in the reduction of properties were seen between the build plate A and build plate C post-heat treatment as well. The heat treatment process however drastically altered the fundamental behavior of the AlSi10Mg transitioning it from a brittle to a semi-ductile metal with a significant increase in ductility of over 400% at the cost of a reduction in the yield and ultimate tensile strengths. For example, heat-treatment of the recommended laser power specimens decreased the yield strength and ultimate tensile strength by 47.7% and 35.5%, respectively. This transition of material properties with heat treatment is well documented in the literature[41–46].

Table 2: Material properties from dog bone tensile specimens of SS 316lL, heat-treated and as-built AlSi10Mg build plate A, B, and C. Heat treatment was two hours at 300°C.

AlSi10Mg	Yield Strength (MPa)	Ultimate Tensile Strength (MPa)	Ductility (%)
SS 316L	511 ± 4	620 ± 4	50.57 ± 0.66
Build Plate A	260 ± 2	380 ± 12	2.95 ± 0.28
Build Plate B	279 ± 2	392 ± 3	2.91 ± 0.08
Build Plate C	243 ± 1	261 ± 4	0.95 ± 0.07
Build Plate A Heat Treated	136 ± 2	245 ± 2	12.66 ± 0.21
Build Plate B Heat Treated	151 ± 0	250 ± 1	13.78 ± 0.41
Build Plate C Heat Treated	130 ± 1	194 ± 1	4.08 ± 0.22

The build plates of SS 316L and AlSi10Mg are shown in Figure 2. The tubular tensile specimens are labeled with the defect type (pristine, P; internal void, IV; quarter crack, QC; through hole, TH) The location of the compression specimen is circled in red and the fracture specimen are boxed in red. The AM notch in the fracture specimens is printed on the top.
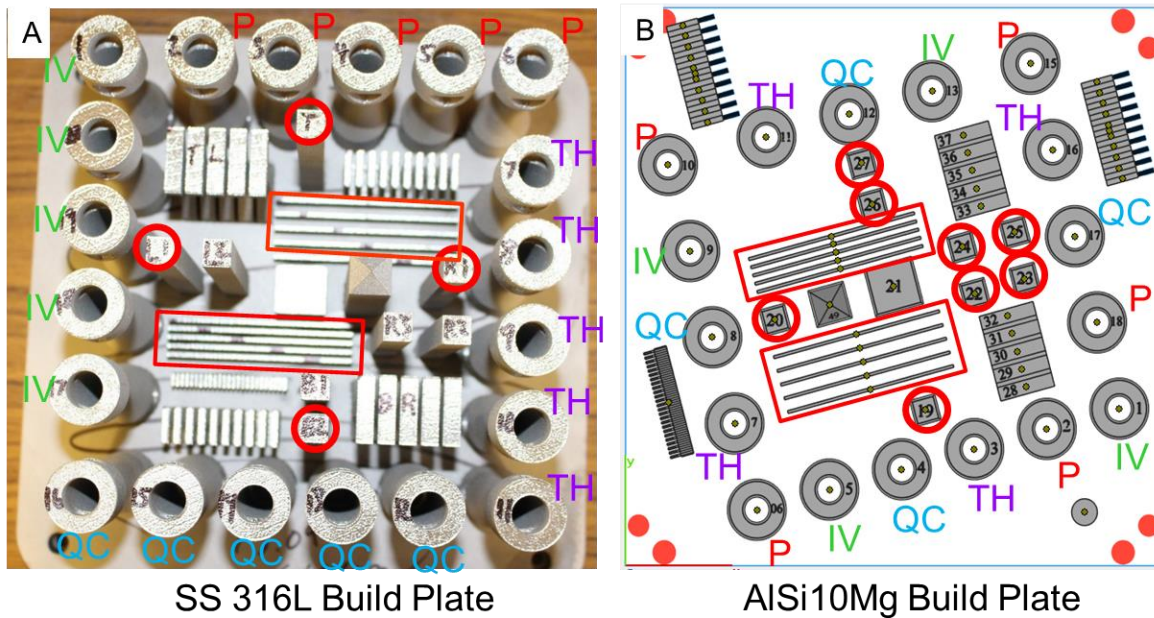
Figure 2: A) AM SS316L build plate layout B) AlSi10Mg build plate layout with Pristine (P), Internal Void (IV), Through Hole (TH) and Quarter Crack (QC) defects in tubular tensile specimens, Compression specimens are circled in red

2.2 Specimens
2.2.1 Tapered Tubular Specimens

Tapered tubular specimens were used in this study to represent the geometry of an engineering component. The tapered tubular tensile specimens were intentionally manufactured with defects (quarter cracks, internal voids, through holes) located in the middle at the thinnest section of the sidewall shown in Figure 3 to demonstrate the effect of a critical geometric flaw in the worst possible scenario. These defects represent potential manufacturing defects (internal voids, quarter cracks) and stress concentrations that may be required for fastening (through hole).
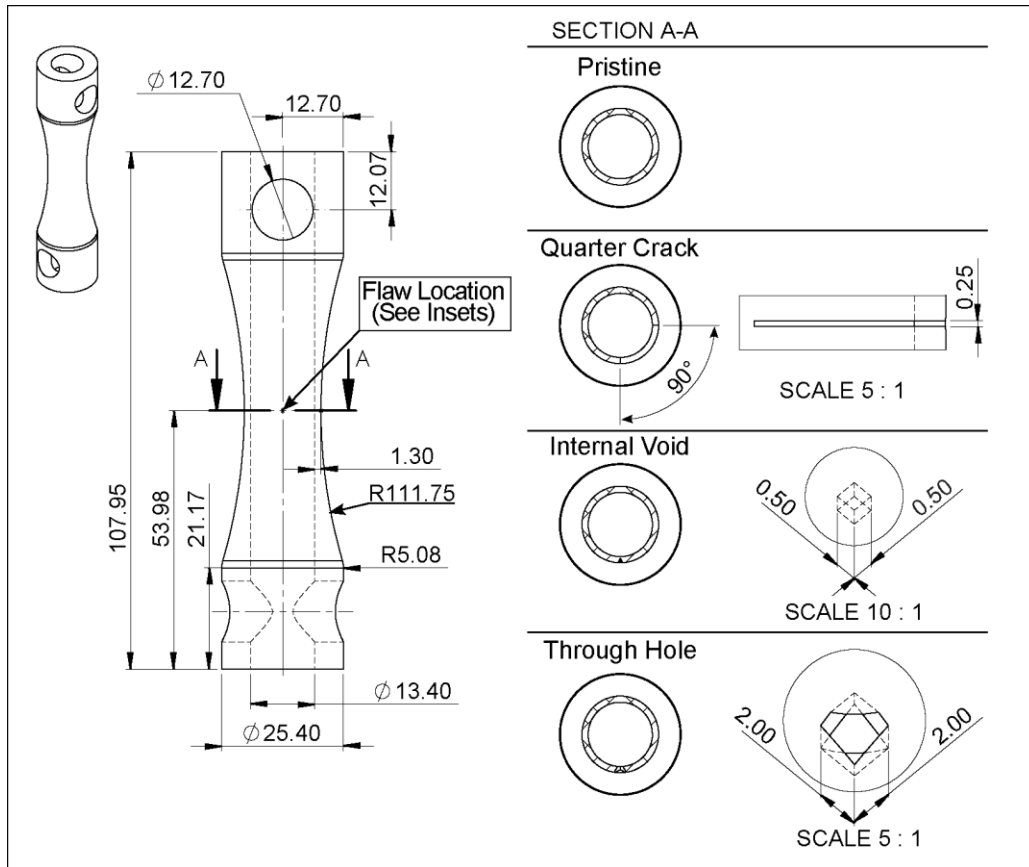
Figure 3: Tubular Tensile Specimens with four types of defects: pristine (no intentional flaw), quarter crack, 0.5mm internal void, 2mm through hole (Image provided by Sandia National Laboratories)

The dimensions of the tubular specimens are shown in Figure 3. Components were printed vertically with the tensile axis aligning with the build direction. These thin-walled exemplary components were designed to mimic typical components being built by AM. The internal void and through-hole defects were printed in a diamond shape (see Figure 3) to avoid steep overhangs thus support material was not required. As a consequence, the internal void and through-hole defects had significantly sharper radii for stress concentration than if they were sphered.

2.2.2 Fracture Toughness Specimens
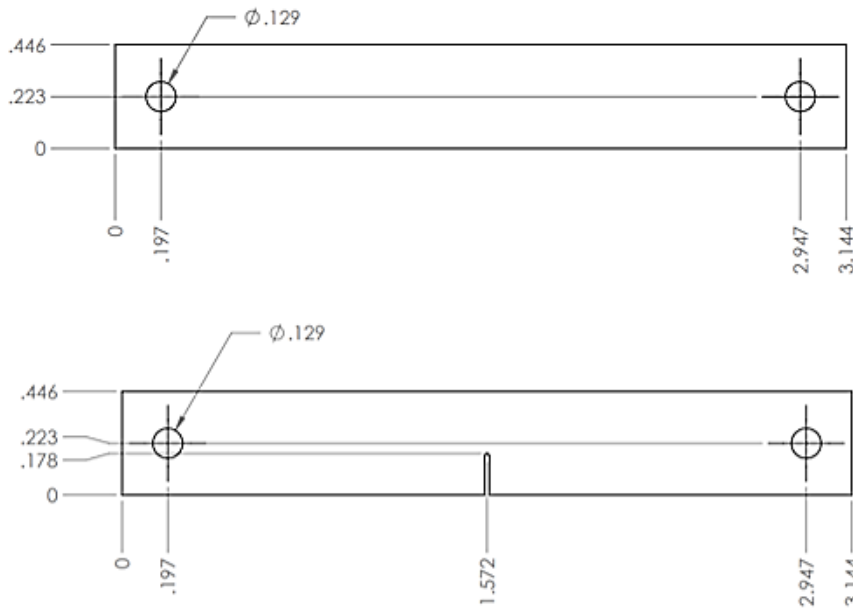
Figure 4: Fracture toughness specimen dimensions (inches)

AM SS 316L and AM AlSi10Mg fracture toughness specimens were manufactured to dimension in Figure 4. These fracture toughness specimens were not designed to ASTM standard E399, because of the space on the build plate [47]. The specimens did not meet the standard for the straight-through wide notch because the crack tip angle was greater than 90°. The specimen also did not meet the standard for a straight-through narrow notch, because the crack width was too large relative to the specimen width. The fracture toughness testing procedure closely followed the ASTM standard E399 [47]. The two notch types included an AM notch and a diamond saw notch. Specimens were notched to approximately 40% of the width using a diamond saw. Pre-cracking was performed on some as the specimen to achieve an a/W (notch plus crack length/specimen width) of 0.45 to 0.55 as stated in the ASTM standard E399 [47]. Half of then AlSi10Mg fracture

toughness specimens were heat treated. The reported fracture toughness values are not standard values for the AM 316 SS and AlSi10Mg but are still useful in studying as a comparison of how notch types and how heat treatment and porosity of AlSi10Mg affect the fracture behavior by comparing their effective fracture toughness values to each other.

2.2.3   Compression Specimens

AM SS 316L and AM AlSi10Mg bars with a cross-section of 10 mm by 10 mm with an approximate length of 100 mm were manufactured. Each of the SS 316L bars and AlSi10Mg bars were machined into five 20 mm long sections for the desired length ratio of 2:1. The build plate location of the bars is circled in red in Figure 2. For both the AlSi10Mg and SS 316l compression specimens, the section closed to the build plate was labeled "1" and the furthest section from the build plate was labeled "5".   The specimens were machined and leveled to 0.0005'' with the accordance with ASTM standard E9-9 [48].

3.   Chapter 3. Experimental Methods

3.1 Tubular Tensile Specimens

Monotonic tensile tests were performed on an MTS Landmark 370 hydraulic load frame with a 100 kN load cell. Experiments were performed in displacement control at a rate of 50 μm/s for SS 316L and 20 μm/s for AlSi10Mg until failure. Different strain rates were used to ensure ample data points were collected because SS 316L was more ductile than AlSi10Mg. Five SS 316L specimens were tested for each defect type. Three as-built and one heat-treated AlSi10Mg specimens were tested for each defect type and build plate.

Clevis grip adaptors with 12.7 mm diameter pins were used to hold the specimen due to the specimen geometry.

Figure 5: Tubular tensile specimen experiment setup with MTS Landmark load Frame and digital image correlation

The elongation and strain fields were measured using 2D DIC. VIC-Gauge 2D software by Correlated Solutions with a virtual extensometer was used to collect the images for DIC. The two ends of the virtual extensometer were placed at the end of the tapered section of the specimen. The virtual extensometer gauge length ranged from 890 to 948 pixels and a pixel area subset of 121 pixels at the ends. A point grey model GS3 camera was used to capture images at 750 ms intervals. The camera was equipped with a Schneider Kreuznach Xenoplan lens model 1001960. The images taken with DIC had a resolution of 2448 x 2048 pixels. The surface roughness of the tubular specimen provided enough contrast for DIC without the need for an applied speckle pattern. Two bright LED lights were used to provide adequate lighting for DIC shown in

Figure *5*.

Fractography was performed at Clemson University's Advanced Materials Research Laboratory with a Hitachi SU 6600 SEM. Images were taken with accelerating voltages of 20 kV. The fracture surface was examined on both SS 316L and AlSi10Mg tubular tensile specimens for each type of defect and build plate.

3.2 Fracture Toughness Testing

Fracture toughness testing was performed using a MTS Landmark load frame. Pinhole grips were inserted to the hydric grips on the load frame. The specimens were loaded into the grips by lining up the specimen with the top pinhole grips and inserted a pin. The actuator was moved up to align the bottom pinhole grip with the specimen. After both pins were inserted into place, the load frame was set to load control of 0 N to make sure there was no accidental loading on the specimen when tightening the plate on the pinhole grips. Plates on the pinhole grips were used to friction clamp the fracture specimen.

In order to measure the fracture toughness, monotonic tensile experiments were performed for each test with a known crack length. This crack length was measured by taking the length of the crack in pixels and using the resolution of the point grey model GS3 camera with a Navistar lens to obtain the crack length in meters. The initial notch and crack were additionally measured after fracture using a microscope. The monotonic tensile tests were performed in displacement control at a rate of 60 μm/s, or a strain rate of approximately 10^{-3} s^{-1}. An initial monotonic tensile test was run to establish a baseline for the strength of the AM notch specimens. In order to test both the effect of an AM notch on

the fracture toughness compared to a diamond saw notch, and the effect of pre-cracking on the fracture toughness compared to initial notches without pre-cracking, four types of tests were performed: diamond saw notch (DS), diamond saw notch with pre-crack grown, AM notch, and AM notch with pre-crack grown. Diamond saw notches were cut into the middle virgin AM SS 316L and AlSi10Mg specimens (same locations as AM notch specimens) to a length of approximately 40% of the width of the specimen. A monotonic test on a diamond saw notch specimen was first performed. This established both an expected value for fracture toughness of notched specimens and a baseline for the expected maximum load that the notched specimens could handle. The SS316L fracture toughness testing was performed by Joby Bartanus [49]. The resulting maximum stress was approximately 700 MPa for SS 316L and 190 MPa for AlSi10Mg. Using this maximum load, a value of 350 MPa for SS316L and 95 Mpa for AlSi10Mg (50% expected max load) was determined to be used as the max cyclic loading of specimens. Pre-cracking of the specimen was performed by cyclically loaded at an R-value of 0.1 between 35 MPa and 350 MPa for the SS316L and 9.5 MPa and 95 MPa or AlSi10Mg to ensure incidental compressive loading was avoided. This was done for the diamond saw and AM notch pre-cracked specimens while viewing the end of the notch through a camera until the crack tip grew and the total crack length reached between 0.45W and 0.55W, according to ASTM standard.

3.3 Compression Testing

Compression tests were performed using a MTS Land Mark load frame. Platen grips were manufactured and inserted into the hydraulic collets for the use of the compression tests with the dimensions (inches) shown in Figure 6.
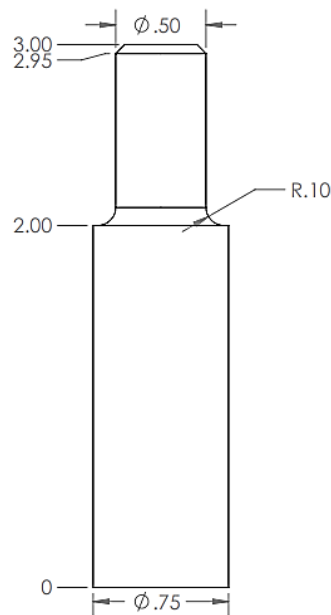
Figure 6: Compression platen tooling dimensions (inches) used in compression testing

The faces of the grips were leveled to 0.0005'' as specified in ASTM standard E9-09 [48]. Each specimen was placed in the center of the bottom grip with the side of the specimen parallel to the camera face. The actuator was slowly raised until just touching the top grip. A digital extensometer was setup using Vic-Guage-2D software to collect strains throughout the experiments. Each compression experiment was performed in displacement

control at 20 µm/s to a compressive strain of approximately 10%. A point grey model GS3 camera was used to capture images at 500 ms intervals. The images taken with DIC had a resolution of 1900 x 1200 pixels. The rough surface finish from the additive manufacturing process on the tubular specimen provided enough contrast for DIC without the need for an applied speckle pattern. The testing of the 4 top and 4 bottom sections of the SS 316L compression specimens was performed by Jody Bartanus [49]. Two bright LED lights were used to provide adequate lighting for DIC.

4. Chapter 4: Results

4.1 Tubular Tensile Specimen Results

4.1.1   SS 316L Tubular Tensile Specimens Results
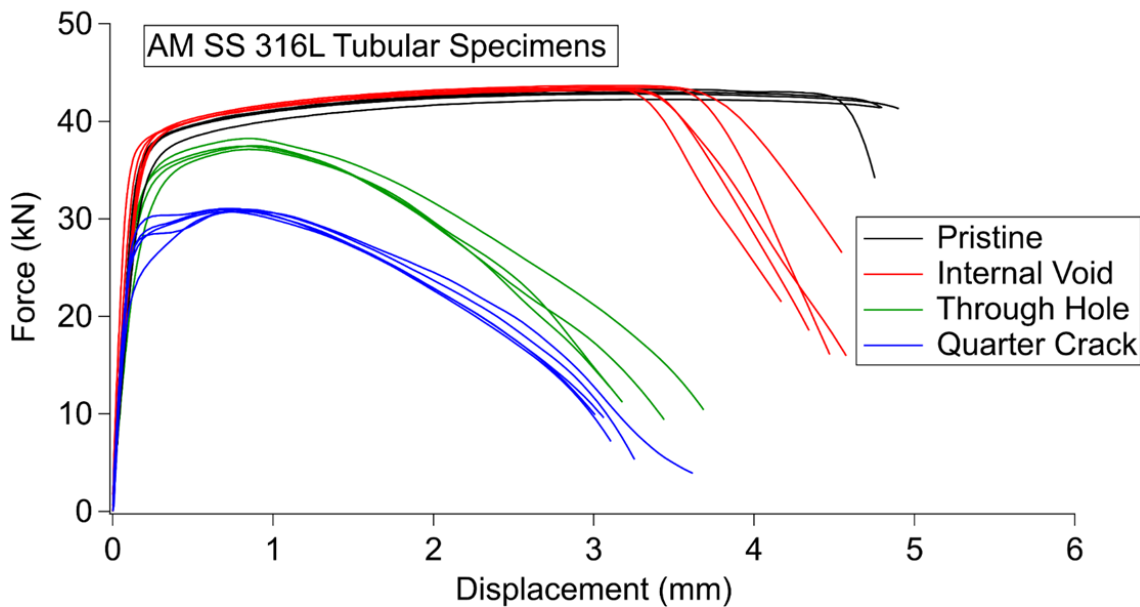
Figure 7: Force-displacement results for SS 316L tubular specimen with intentionally manufactured defects in the sidewall.

Force/displacement results of tensile tests on all SS 316L tubular components are displayed in Figure 7. The flawed specimens exhibited ductility and softening after peak load. The pristine specimen exhibited less softening before failure. Tubular specimens with internal voids had similar strength to the pristine specimens with an average maximum force of 43.47 ± 0.15 kN compared to 42.90 ± 0.42 kN. The internal void in the SS 316L specimens decreased the overall ductility of the component, resulting in a reduction of 6% average elongation compared to the pristine counterparts, reducing from 5.01 ± 0.22 mm to 4.71 ± 0.27 mm.   Quarter crack specimens were the weakest with an average maximum force of 31.12 ± 0.22 kN followed by the through-hole specimens with an average maximum force of 38.01 ± 0.71 kN. During testing, the quarter crack specimens had an audible 'pop' when the quarter crack opening up and a drop in force was measured.   The overall decrease in elongation to failure of samples containing these two flaws were significant compared to the pristine case and ranged between 3 to 4 mm. Overall, intentionally manufactured defects decreased the strength and ductility in AM SS 316L tubular tensile specimens. The reduced strength and ductility correlated to a reduction in cross-sectional area from each defect starting with pristine, internal void, through hole and quarter crack which was the weakest and least ductile.

4.1.2   AlSi10Mg Tubular Tensile Specimen Results
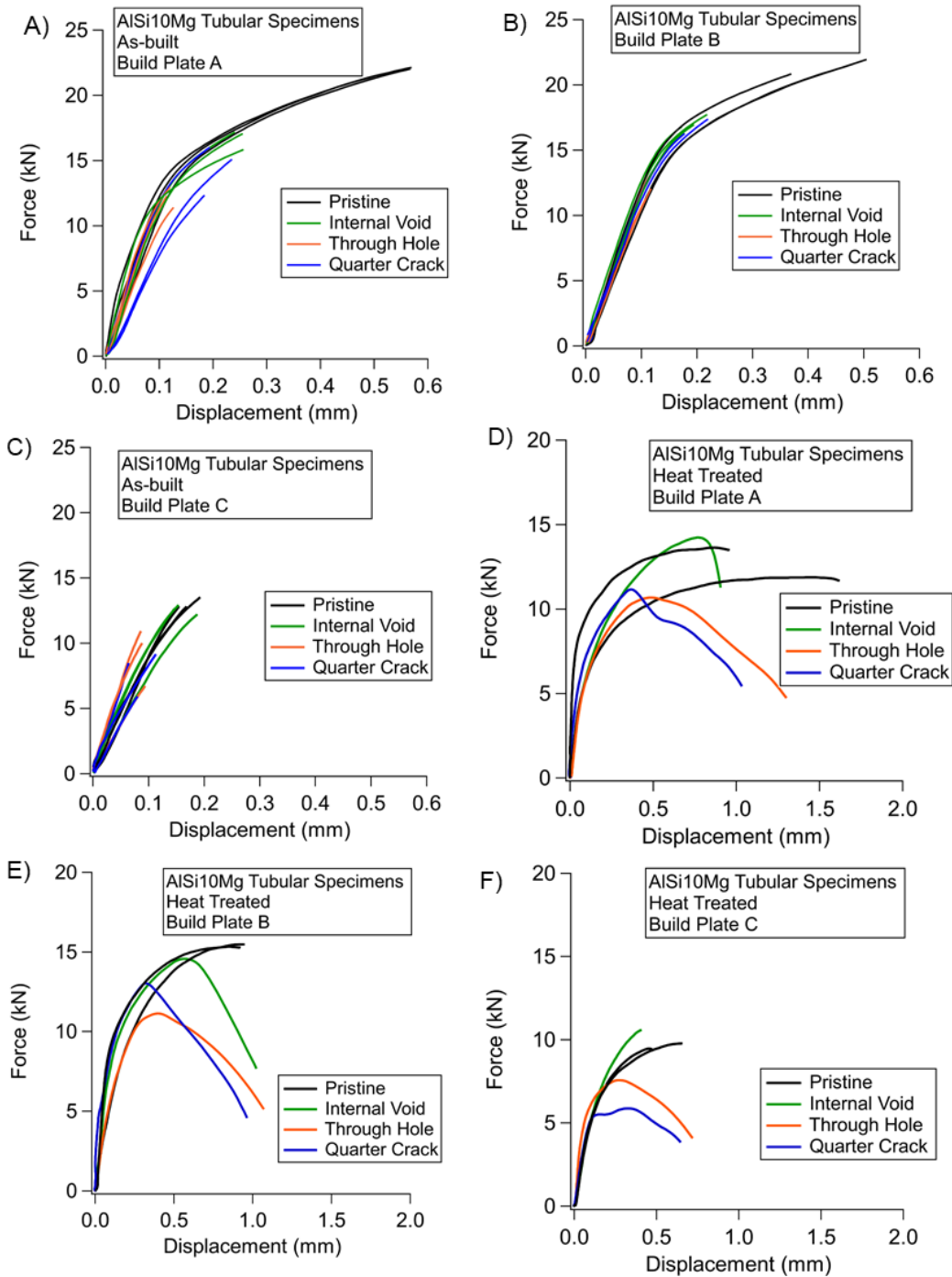
Figure 8: AlSi10Mg force-displacement results for each build plate. A) As-built build plate A AlSi10MG B) As-built build plate B AlSi10Mg C) As-built build plate C AlSi10Mg D) Heat-treated build plate A AlSi10Mg E) Heat-treated build plate B AlSi10Mg F) Heat-treated build plate C AlSi10Mg

The force and displacement results for each type of defect and laser power are shown in Figure 8 for both as-built and heat-treated specimens. The pristine as-built AlSi10Mg had an average maximum force and elongation of 22.27 ± 0.04 kN and 0.586 ± 0.01 mm for build plate A and 13.40 ± 0.34 kN and 0.183 ± 0.02 mm for build plate C. The results showed the addition of the internal void defect only decreased the average maximum force and elongation by 23% and 54% for build plate A, 19 % and 56% for build plate B, and 2.6% and 4.4% for build plate C respectively. The through hole defect in as-built AlSi10Mg decreased the average maximum force and elongation by 43% and 77% for build plate A, 41% and 73% for build plate B, and 27% and 46% for build plate C. The addition of a quarter crack in as-built AlSi10Mg decreased the average maximum force and elongation by 33% and 62% for build plate A, 22% and 57% for build plate A and 37% and 49% for build plate C. Results of the average maximum force and elongation to failure for the test matrix are found in Tables 3 and 4, respectively. From comparing SS 316L and AlSi10Mg in Table 3 and

Table 4, the as-built AlSi10Mg specimens were more negatively affected by defects compared to the SS 316L specimens.

Heat-treatment of AlSi10Mg pristine specimens decreased the average maximum force and increased the average elongation by 42% and 125% for build plate A, 31% and 103 % for build plate B, and 23% and 253% for build plate C, respectively. The addition of an internal void in the heat-treated AlSi10Mg changed the maximum force and the elongation by +12% and -28% for build plate A and -2.3% and +18 % for build plate B, and +3.9% and -33% for build plate C. The through hole in the heat-treated AlSi10Mg changed the maximum force and the elongation by -19% and +2.2% for build plate A, -33% and +17% for build plate B, and by -33% and +24% for build plate C. The quarter crack in the heat-treated AlSi10Mg changed the maximum force and the elongation by -10% and -18% for build plate A, -10% and +4% for build plate B, and by -41% and +10% for build plate C. During the quarter crack specimen experiments, the crack opened with an audible 'pop' and a drop in force was observed, similar to the SS 316L quarter crack specimens.

Table 3: Average maximum force of AlSi10Mg and SS 316L tubular tensile specimens with intentionally manufactured defects in the sidewall

Specimen	Average Maximum Force (kN)			
	Pristine	Internal Void	Through Hole	Quarter Crack
AlSI10Mg Build Plate A	22.27 ±0.04	17.10 ± 0.65	12.74 ± 0.63	14.93 ± 1.54
AlSI10Mg Build Plate B	21.75 ± 0.43	17.61 ± 0.35	12.92 ± 0.85	16.89 ± 0.58
AlSI10Mg Build Plate C	13.40 ± 0.34	13.10 ± 0.17	9.78 ± 1.83	8.36 ± 1.40

SS 316L	42.90 ±0.43	43.47 ± 0.15	38.01 ± 0.71	31.12 ± 0.22

Table 4: Average elongation of AlSi10Mg and SS 316L tubular tensile specimens with intentionally manufactured defects in the sidewall

Specimen	Average Elongation (mm)			
	Pristine	Internal Void	Through Hole	Quarter Crack
AlSI10Mg Build Plate A	0.586 ± 0.01	0.278 ± 0.01	0.136 ± 0.009	0.220 ± 0.024
AlSi10Mg Build Plate B	0.474± 0.06	0.209 ± 0.02	0.127 ± 0.01	0.201 ± 0.03
AlSI10Mg Build Plate C	0.183 ± 0.02	0.175 ± 0.02	0.099 ± 0.004	0.093 ± 0.022
SS 316L	5.01 ± 0.22	4.71 ± 0.27	3.76 ± 0.27	3.68 ± 0.22

Table 5: SS 316L and AlSi10Mg recommended power specimen defects types comparison of cross-sectional area to peak load and displacement

GeometricFeatures	Area (%)	Peak Load (%)		Max Disp (%)	
		SS 316L	AlSi10Mg	SS 316L	AlSi10Mg
Pristine	100	100	100	100	100

Internal Void	99.6	100	77	94	47
Through Hole	96.1	89	56	75	23
Quarter Crack	75	73	67	73	38

Shown in Table 5, SS 316L mechanical behavior was driven by a reduction in the cross-sectional area. The quarter crack SS 316L peak load was 73% of the pristine load with 75% of the area. The through-hole acted as a stress concentration because of the sharp corners and there the decrease in peak load for both SS 316L and AlSi10Mg was greater than the reduction in cross-sectional area. AlSi10Mg is driven more by the stress concentration compared to the AlSi10Mg which follows close to the reduction in cross-sectional area. The maximum displacement for both materials is impacted more by the reduction in the cross-sectional area compared to the peak load.*: Average maximum force of AlSi10Mg and SS 316L tubular tensile specimens*

4.1.3   Tubular Tensile Specimens Fractography Results
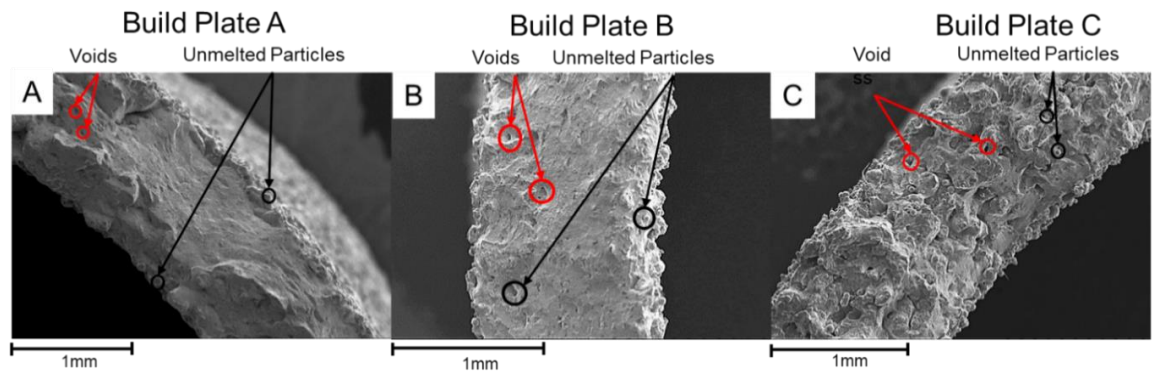
Figure 9: Fractography images of the fracture surface of the as-built AlSi10Mg pristine specimens build plate A, B, and C

In *Figure 9*A, there was a brittle fracture in the build plate A AlSi10Mg and a few identified internal voids and unmelted particles in the interior of the fracture surface. In build plate C in *Figure 9*C, the fracture surface was comprised of voids and unmelted particles. The increase of voids and unmelted particles was seen in all build plate C AlSi10Mg tubular tensile specimens. Reducing the manufacturing laser power resulted in an increase in porosity with a relative density of 94.9% and a decrease in average maximum force by 40% of the recommended power pristine specimens. The increase in porosity in the reduced power negatively affected the strength and ductility of the AlSi10Mg specimens. Build plate B had a relative density of 99.2% and has similar strength to build plate A.
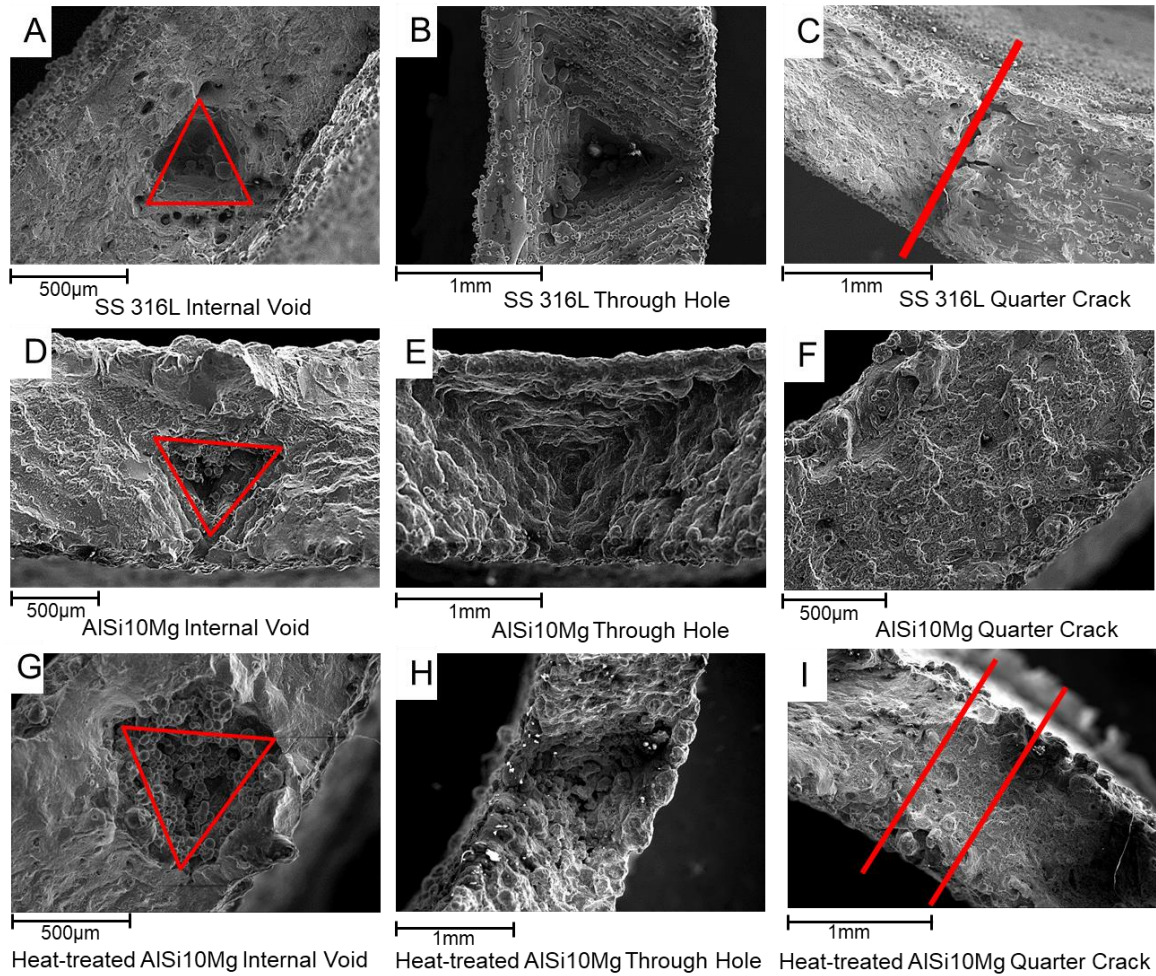
Figure 10: Fractography images of the fracture surface at manufactured defects in SS 316L and build plate A AlSi10Mg specimens A) SS 316L internal void highlighted in the red triangle. B) SS 316 through hole C) SS 316L quarter crack transition line between fracture surface and manufactured quarter crack defect D) AlSi10Mg internal void highlighted in the red triangle E) AlSi10Mg through hole F) AlSi10Mg quarter crack defect surface G) Heat-treated AlSi10Mg internal void highlighted in the red triangle H) Heat-treated AlSi10Mg through hole I) Heat-treated AlSi10Mg quarter crack transition area shown between the red lines
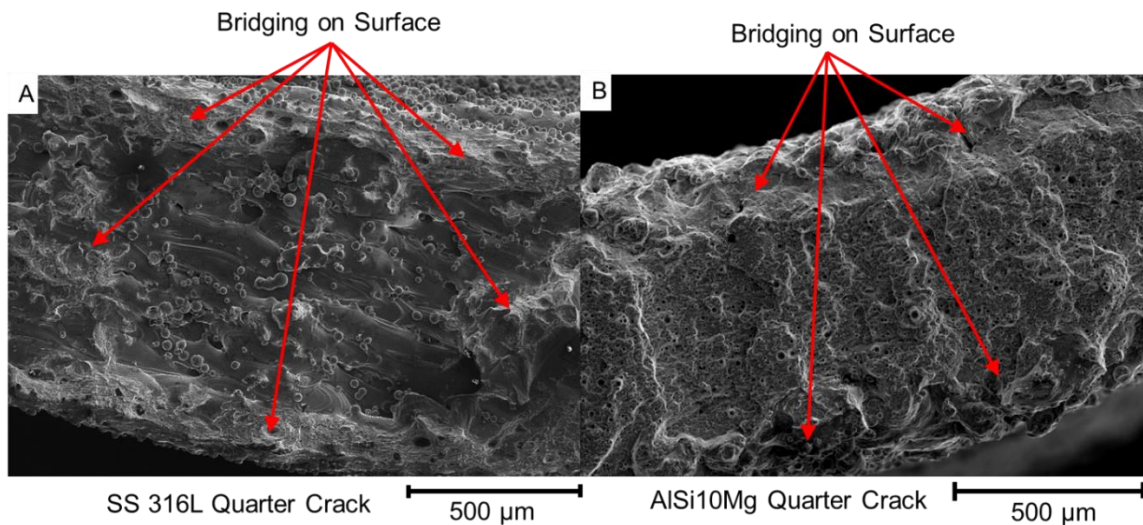
Figure 11: Quarter crack defect surface of SS 316L and AlSi10Mg. Bridging on the quarter crack defects surface is circled in red.

From the fractography images are shown in Figure 10 A-C ductile fracture was observed in the SS 316L specimen evident by the dimpled fracture surface. Indicating brittle fracture sharp ridges on the fracture surface in the AlSi10Mg specimens' fractography was observed. Shown in Figure 10 A and Figure 10 D, the fractography images showed the triangle-shaped internal void on the fracture surface of the SS 316L and AlSi10Mg specimens. The internal void and through hole defects were diamond-shaped to avoid using support material. The diamond-shaped defects had sharp corners that have a higher stress concentration factor than a spherical void. In Figure 10 C, the quarter crack SS 316L specimen, there was a clear transition line between the fractured surface and manufactured quarter crack, indicated by a red line on the micrograph. There is evidence of bridging in Figure 11 A from fracture surfaces on areas of the SS 316L quarter crack

defect surface, and this aligns with the test results. Individual layers from the additive manufacturing process were seen at the fracture surface of the internal void and through hole defects, in Figure 10 A, B, D, E, G, H. Unmelted particles were seen on all of the defect fracture surfaces in both SS 316L and AlSi10Mg. The image shown in Figure 10 F specifically showed the unmelted particles on the quarter crack defect, and there is evidence of bridging in Figure 11 B from fracture surfaces on areas of the AlSi10Mg quarter crack defect surface.
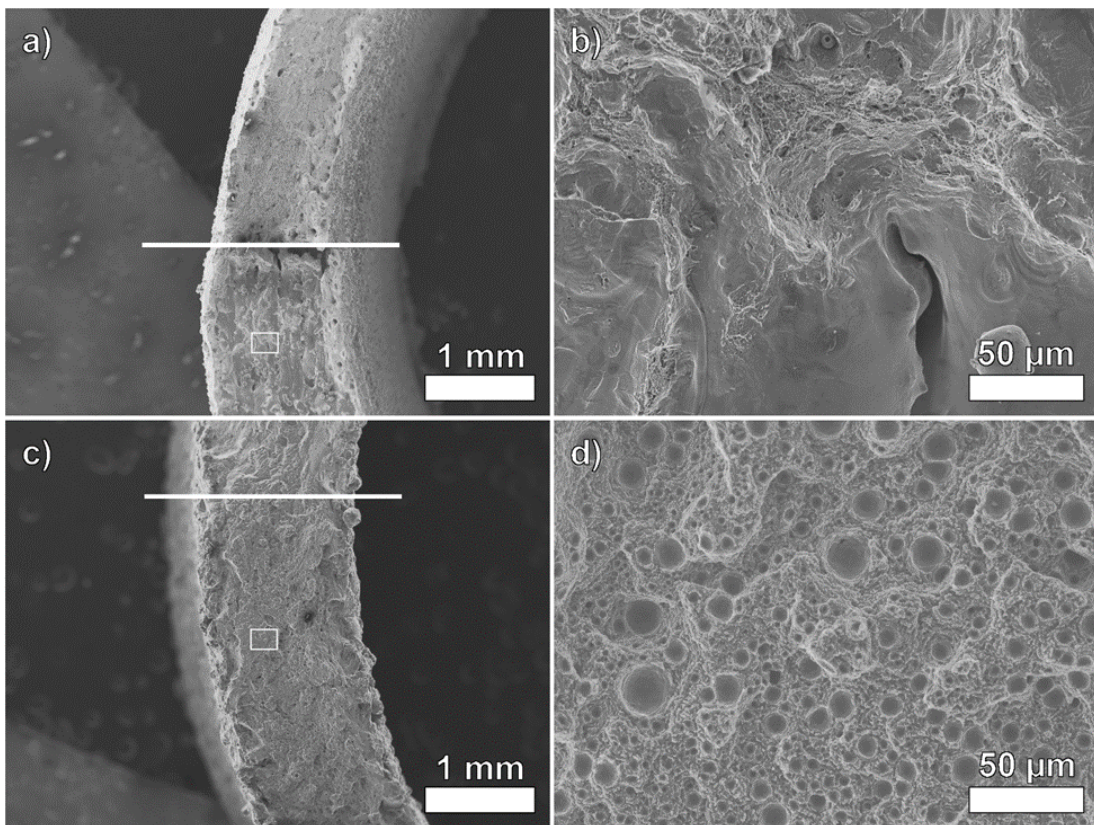
Figure 12: SEM secondary electron micrographs of a quarter crack sample for the (a,b) stainless steel and (c,d) AlSi10Mg build plate A The white line in the left column approximates the end of the printed flaw. Insets in the printed flaw region are highlighted in the boxes of the right column which are shown in detail in the left column. (Images were taken by Sandia National Laboratories)

The introduction of the quarter crack was effective in the SS 316L with minor bridging seen in the flat regions in Figure 12A and B. Shown in Figure 12C and D, the quarter crack in the recommended power AlSi10Mg had a significant amount of bridging between the layers. Shown in Figure 12D, AlSi10Mg appeared to have an increase in gas bubbles on the surface compared to the SS 316L. Gas bubbles are usually formed internally below the surface when there is a high solidification rate and there is not enough time for the gas bubble to rise and escape from the surface [50,51]. The gas bubbles on the quarter crack defect surface indicate the gas could not escape and the surface was bridged between layers. The increases in the bridging of the AlSi10Mg quarter crack could help explain why the quarter crack specimens were stronger than the through hole specimens.

The bridging in the AlSi10Mg quarter crack became more apparent with the increased ductility from the heat treatment. During testing of the heat-treated AlSi10Mg and SS 316L, there was a decrease in force and noticeable noise from the quarter crack opening. The results of the as-built AlSi10Mg did not see a drop in force and the quarter crack did not open before failure. There was bridging in all of the quarter crack specimens. Images in Figure 12 shown there was more bridging on the quarter crack defect surface of AlSi10Mg compared to SS 316L. The difference in bridging effects in AlSi10Mg and SS 316L was due to different material properties and the amount of bridging from the manufacturing.
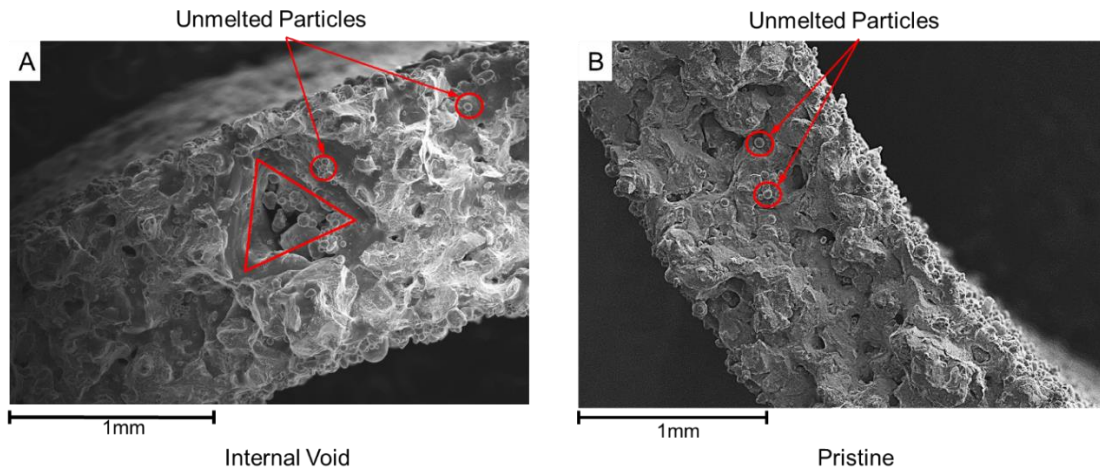
Figure 13: Fractography images of AlSi10Mg build plate C comparing internal void and pristine specimens.

The internal void in *Figure 13* A was surrounded by unmelted particles and voids. The fracture surface in *Figure 13* B of the pristine build plate C showed a fracture surface abundant with voids and unmelted particles similar to the internal void defects in the reduced power. The fractography in *Figure 13* highlights that increased porosity in AM materials can start to dominate the material structure over other types of defects. The increased porosity in build plate C AlSi10Mg decreased the impact of the interval void defect. Shown in Table 3 and

Table 4, the introduction of geometric defects in the build plate C AlSi10Mg build plate had a smaller percentage decrease in average maximum force and elongation compared to the recommended power AlSi10Mg build plate.

4.2 Fracture Toughness Results

Table 6: AM SS316L Fracture Toughness Results (Results from Jody Bartanus [49])

AM SS316L Fracture Toughness Tests		
Experiment	# of Specimens	K_{IC} (MPa-m$^{1/2}$)
Diamond Saw Notch, No Pre-cracking	1	85.80
Diamond Saw Notch, Pre-cracking	3	108.73-110.83
AM Notch, No Pre Cracking	1	79.61
AM Notch Pre-cracking	1	126.12

The fracture toughness was calculated using a stress intensity factor for a single edge notch in tension from the equations below [52].

$$K_I = \sigma\sqrt{\pi a} \cdot F_I(\alpha) \ , \ \ \alpha = \frac{a}{W} \ \ , \text{ where a is total notch and crack length, W is width}$$

$$F_I(\alpha) = 1.12 - 0.231\alpha + 10.55\alpha^2 - 21.72\alpha^3 + 30.39\alpha^4$$

Shown in Table 6 pre-cracking the SS 316L resulted in higher fracture toughness. AM and diamond saw notches for SS 316L had similar fracture toughness.

Table 7: AM AlSi10Mg Fracture Toughness Results Heat Treated

AM AlSi10Mg Fracture Toughness Heat Treated			
Build Plate	Notch Type	# of Specimens	K_{IC} (MPa-m$^{1/2}$)
Build Plate A	AM	1	31.75
Build Plate A	DS	2	26.21 - 26.68
Build Plate A, no pre-cracking	DS	1	23.41
Build Plate B	AM	1	30.26
Build Plate B, no pre-cracking	AM	1	28.21
Build Plate B	DS	2	27.49 - 29.85
Build Plate C	AM	2	22.80-23.23
Build Plate C	DS	2	22.01-23.47

The diamond saw notch and AM notch for heat-treated AlSi10Mg shown in Table 7 had similar fracture toughness when comparing each build plate separately. The

increased porosity with AlSi10Mg build plate C had a negative impact on the fracture toughness. AlSi10Mg build plate A and B for both diamond saw and AM notch had similar fracture toughness.

Table 8: AM AlSi10Mg Fracture Toughness As-Built Results

AM AlSi10Mg Fracture Toughness As-Built			
Build Plate	Notch Type	# of Specimens	K_{IC} (MPa-m$^{1/2}$)
Build Plate A	AM	2	27.93 - 30.13
Build Plate A	DS	2	29.58 - 30.94
Build Plate B	AM	2	31.01 - 31.72
Build Plate B	DS	2	28.25 – 32.68
Build Plate C	AM	2	21.11 - 22.83
Build Plate C	DS	2	20.37 - 22.26

The heat treatment of AlSi10Mg appeared to not have a significant impact on the fracture toughness for all three build plates. For both the heat-treated and as-built AlSi10Mg fracture specimen the AM notch and DS notch had similar results. Shown in Table 7 and Table 8 there was a decrease in the fracture toughness from build plate A to

build plate C in both the as-built and heat-treated. With an increase in porosity and the

fracture toughness decreased.

4.3 Compression Results

Table 9: AM SS 316L Compression Results (section 5 is furthest from the build plate and section 1 is the closest to the build plate.)

AM SS 316L Compressive Testing									
	Compressive Modulus (GPa)					Compressive Yield Stress (MPa)			
Specimen	5 (Top)	4	3	2	1 (Bot)	5 (Top)	4	3	2	1 (Bot)
R1	122	153*	153	144*	132	440	475*	492	488*	462
B2	131	134	162	161	145	441	469	504	508	524
T	121	121	156	156	156	424	428	502	516	506
L1	145	143	163	157	162	465	488	522	504	520

*Grips slipped during testing

The AM SS 316L compression results in Table 9 show the compressive modulus

and yield strength decreases as the distance above the build plate increases. The first three

sections closest to the build plate of compression specimens B2, T, and L1 had similar

compressive modulus and compressive yield strength. Specimen L1 was the strongest

specimen with an average compressive yield strength of 500 MPa compared to R1, B2, and

T with 465 MPa, 489 MPa, and 475 MP.

Table 10: AM AlSi10Mg Compression Results (Section 5 is the furthest from the build plate and section 1 is the closest to the build plate) All specimens heat-treated at 300 °C for 2 hours

AM AlSi10Mg Compressive Testing									
	Compressive Modulus (GPa)					Compressive Yield Stress (MPa)				
Specimen	5 (Top)	4	3	2	1 (Bot)	5 (Top)	4	3	2	1(Bot)
20-A	66.3	77.7	72.3	79.4	79.1	189	187	184	189	191
23-A	72.7	80.9	69.4	67.6	82.2	193	188	187	186	193
25-A	69.5	76.3	69.3	69.6	68.5	160	168	164	165	165
27-A	74.7	77.6	66.2	65.9	79.3	168	164	163	162	166
19-B	84.8	68.1	70.8	78.8	65.6	191	192	191	189	197
22-B	63.4	65.2	68.3	72.4	57.1	174	171	170	172	173
24-B	73.1	66.7	66.5	67.1	59.3	172	168	173	164	166
26-B	69.5	65.6	62.3	79.3	66.3	175	170	170	170	169

In Table 10, Specimen 20-A and 23-A were significantly stronger than 25-A and 27-A. The yield strength of the AlSi10Mg remained consistent across all the AlSi10Mg compression sections regardless of build height. The compressive yield modulus for the

AlSi10Mg compression specimens fluctuated from each section. There was not a clear trend of certain sections in AlSi10Mg having increased material properties. Specimen 19-B had an average compressive yield strength of 192 MPa and was significantly stronger than 22-B, 24-B, and 26-B with an average yield stress of 172 MPa, 169 MPa, and 171MPa. Specimen 25-A and 27-A had similar strength to specimens 22-B, 24-B, and 26-B. Build plate A and B had similar compression properties.

5. Chapter 5: Discussion

5.1 Relationship of Defects and Ductility

Ductile fracture was seen in the fracture surface of the SS 316L specimens and brittle fracture was seen in the as-built AlSi10Mg specimens. The internal void defects had a larger impact on the mechanical properties of as-built AlSi10Mg compared to SS 316L. As the ductility of the AM metals increased, the impact of the geometric defects decreased. The heat treatment of AlSi10Mg begins to shift the defect dependence from geometry to cross-sectional area dependence. This relationship between ductility and stress concentrations is outlined in literature for traditional metals and can be applied also AM materials [11]. Brittle materials are generally more sensitive to crack growth and are more negatively affected by geometric defects compared to ductile materials [11,53].

The through hole was weaker than the quarter crack for the as-built AlSi10Mg specimens. This was most likely due to the through hole, acting as a stress concentrator, having sharp corners and the brittle materials having increased sensitivity because of their lack of hardenability. With a higher ductility, such as in the SS 316L, the reduction in the

cross-sectional area becomes the driving factor and the quarter crack becomes weaker than the through hole.

SS 316L and heat-treated AlSi10Mg both exhibited ductile failure. When the quarter cracks opened during testing the SS 316L and heat-treated AlSi10Mg specimens, the specimens plastically deformed, stain hardened and continued to support loading. In comparison, the as-built AlSi10Mg specimens fractured when the quarter crack opened. Gas bubbles, which are usually only seen below the surface, were seen in the AlSi10Mg quarter crack defect surface and are an indicator of bridging. The combination of bridging, sharp corners in the through hole, and a defect transition region is likely the reason the through hole was weaker than the quarter crack in the AlSi10Mg as-built components.

From this study, AM AlSi10Mg and SS 316L follow traditional knowledge on mechanical behavior with stress concentration and ductility. An increase in the ductility of an AM metal decreases the influenced of geometric defects. A previous study characterizing the effect of pore size on tensile properties of AM SS 316L aligned well with the AM SS 316L internal void results in the present study [54]. The internal void saw similar strength to the pristine specimen, but a small decrease in elongation. The results for both SS 316L and AlSi10Mg tubular specimens agree with the findings of the elongation to failure is more sensitive than strength with respect to the size of the defect. In **Error! Reference source not found.**, the SS 316L peak load was driven by a significant reduction in the cross-sectional area again agree with Wilson-Heid *et al.* [54].

5.2 Defect and Porosity Relationship

Distinct material behaviors for each build plate have been seen in AlSi10Mg tubular specimens. The mechanical behavior of the as-built AlSi10Mg build plate A in Figure 8A was driven by the type of defect because each group of defects displayed similar mechanical behavior. The mechanical behavior of the as-built build plate B shown in Figure 8B was driven by the presence of a defect because the results were closely grouped together and differ by the presence of a defect. The mechanical behavior of the as-built built plate C AlSi10Mg shown in Figure 8C showed reduced ductility and lower strength than the build plate A results. In the build plate C specimens, porosity dominates the overall mechanical behavior. Fractography images in *Figure 13* and results in Figure 8 C and D further support the conclusion that porosity began to dominate over the geometric defects in build plate C AlSi10Mg. There is a clear trend in the AlSi10Mg as-built and heat-treated specimens. As the relative density decreases, the porosity starts to dominate the material behavior over the other intentionally manufactured defects. The results from the AlSi10Mg specimens agreed well with a large study on the relationship between porosity and strength of copper made from binder jetting additive manufacturing [55].

There have been separate studies on the effect of porosity [55] and the effect of pore size [54] on the mechanical behavior of AM metals, but the combination of porosity and geometric defects in AM metals has not been fully explored. A critical porosity-defect relationship is needed to qualify components for safe use. From this study, AM 316L and AM AlSi10Mg, in brittle and ductile forms, follow convectional knowledge about stress

concentrations and the results have an agreement with other studies on porosity and pores size for AM metals.

5.3 AM and DS Notch Fracture Toughness

For both AlSi10Mg and SS 316L, there was no significant difference in fracture toughness between the AM and DS notch for the single edge notch tensile specimens. The fracture toughness of a notch manufactured during SLM was similar to a notch made in a post-manufacturing process. In the AlSi10Mg build plate, C the increase in porosity decreased the fracture toughness. This reinforces the conclusion of increased porosity will start to dominate the mechanical behavior.

The fracture toughness of die-cast AlSi7Mg ranges from $18 - 29$ MPa$\sqrt{m}$ depending on heat treatment composition [56]. The results of AlSi10Mg are on the upper range to the fracture toughness of die-cast AlSi7Mg. The fracture toughness of the die-cast AlSi7Mg was calculated for a plane strain case. Apparent fracture toughness is dependent on the thickness of the specimen[11]. As the thickness decreases, the apparent fracture toughness increases and becomes closer to a plane stress case.. The AlSi10Mg results at agrees with literature that apparent fracture toughness increases with a decrease in thickness. For a ductile fracture of metals, the crack grows through the center of the specimens. The crack growth of the edges lags behind the center and occurs at a 45° angle to the applied load. The fracture surface has a flat surface in the middle and 45° shear lips on the edges[11]. With thinner ductile specimens, the shear lips make up a larger area of the fracture surface

and have an impact on the apparent fracture toughness [11]. Understanding fracture toughness for thin AM components is important because thin and complex sections can be made using AM to save weight, cost, and manufacturing time Further research will be needed to fully understand the fracture toughness of thin AM components

. .

5.4 Effect of Build Plate Height and Location

The SS 316L compression results show that as the distance from the build plate increased the compressive modulus and compressive yield strength decreased. This occurs because as the distance from the build height increased the grain size increase [30,31]. The Hall-Petch relationship defines an inverse relationship between grain size and yield strength[10,53,57]. Observation from a study on AM SS 304 [10] showed large grain sizes near the build plate, resulting in increased material properties following the Hall-Petch relationship.

The AlSi10Mg compression results did not show an increase in material properties at the sections closet to the build plate. The compression material properties of AlSi10Mg shown in Table 10 were constant across the sections of each compression column. Compression specimens in build plates A and B had similar material properties. The material properties of SS 316L were clearly dependent on the distance from the build plate, compared to AlSi10Mg, which has similar material properties as each distance. A study [9] on the build height on Inconel 718 produced by SLM observed there was no obvious changing trend along the build heights of the components. From the results of the SS 316L

and AlSi10Mg compression specimens, the effect of build height is material dependent and this aligns with findings in literature for various materials [9,10].

The material properties of the AlSi10Mg and SS 316L compression specimens also varied by the location on the build plate. Specimens 20A and 23A were significantly stronger than 25A and 27A. Specimen 19B was significantly stronger than 22B, 24B, and 26B. Looking at the build plate locations of the AlSi10Mg compression specimens shown in Figure 2 B, specimen 19B and 20A are on the opposite side of the build plate from other compression specimens. Specimen 23A near the other compression specimen but had similar material properties as 20A. Compressive material properties varied by build plate location, but there is not a clear trend between build plate location and increased material properties.

6. Chapter 6: Conclusions

Three distinct structural behaviors were observed in the AM AlSi10Mg build plates. As porosity increased in the AlSi10MG tubular specimens, the mechanical behavior changed from being driven by the type of geometric defect to being driven by the increased porosity. Porosity in the build plate C AlSi10Mg build plate overwhelmed the intentionally manufactured flaws. Heat treatment of AlSi10Mg increased the ductility, thus reduced the effect of the defects on material behavior. Heat-treated AlSi10Mg and SS 316L both exhibited ductile failures that are seen with typical ductile metals. In all material testing conducted in this study, intentionally manufactured defects decrease the strength and

43

ductility. As-built AM AlSi10Mg was more sensitive to defects compared to AM SS 316L and saw a larger decrease in strength in ductility. Materials behavior for a ductile AM SS 316L and a brittle AM AlSi10Mg were similar when compared to brittle and ductile wrought metals.

The mechanical behavior of the brittle AM as-built AlSi10Mg was driven by geometric defects acting as stress concentrations. The mechanical behavior of the ductile AM SS316L was driven by geometric defects reducing the cross-sectional area. From this study, AM AlSi10Mg and AM SS 316L followed traditional facts about stress concentrations and ductility for metals. The results from this study give the initial steps to determining a critical porosity-defect relationship of AM metals for safe use. Interaction between natural flaws and the intentionally manufacture flaws could have had a negative impact on the structural behavior on the AM components.

7. Chapter 7: Future Works

From this study, AM SS 316L and AM AlSi10Mg, in brittle and ductile forms, follow convectional knowledge about stress concentrations and the results have agreement with other studies on porosity and pores size for AM metals. Further testing and analysis with other AM metals, defects sizes, and porosity levels will be needed to fully define the relationship between defects and porosity, but these results can assist in the initial steps. Beyond this study, the shape and network of the pores may prove to be just as important. Uneven porosity near geometric defects can affect the mechanical behavior and could have been a contributing factor in this study. This study is the first step to establish a defect-porosity relationship to qualify AM components for safe-use.

AlSi10Mg build plate A and B had very similar strength and ductility compared to build plate C. A future investigation to laser power levels between build plates B and C would help define the porosity level when the mechanical behavior starts to be dominated by the decrease in relative density.

Three distinct behaviors were observed in AlSi10Mg. SS 316L could be tested at these increased porosity levels to determine if these behaviors are seen in another material that is more ductile. Further exploration into the grain structure could explain why build plate B was slightly stronger than build plate A.

Additional testing of thickener AM specimens will help further define the relationship for fracture toughness of thick and thin AM components. The focus of a further fracture study would be investigating the influence of the specimen thickness on the apparent fracture toughness. The microstructure of thick and thin AM parts is different because of the rate of cooling and the manufacturing process.

The compression tests reveal the build height affects the material behavior. A further studied investigating the on the microstructure and grain size using electron backscatter diffraction at each build height and location would help determine why SS 316L showed an increase in material properties while AlSi10Mg was constant across all the sections.

REFERENCES

[1]   Tofail SAM, Koumoulos EP, Bandyopadhyay A, Bose S, O'Donoghue L, Charitidis C. Additive manufacturing: scientific and technological challenges, market uptake and opportunities. Mater Today 2018;21:22–37. doi:10.1016/j.mattod.2017.07.001.

[2]   Liu B, Kuai Z, Li Z, Tong J, Bai P, Li B, et al. Performance Consistency of AlSi10Mg Alloy Manufactured by Simulating Multi Laser Beam Selective Laser

Melting (SLM): Microstructures and Mechanical Properties. Materials (Basel) 2018. doi:10.3390/ma11122354.

[3]   Wohlers Associates 2019 state of 3D printing report published - 3D Printing Industry n.d. https://3dprintingindustry.com/news/wohlers-associates-2019-state-of-3d-printing-report-published-152117/ (accessed October 9, 2019).

[4]   Leach RK, Bourell D, Carmignato S, Donmez A, Senin N, Dewulf W. Geometrical metrology for metal additive manufacturing. CIRP Ann - Manuf Technol 2019. doi:10.1016/j.cirp.2019.05.004.

[5]   ASTM F3049 Standard Guide for Characterizing Properties of Metal Powders Used for Additive Manufacturing Processes. n.d. doi:10.1520/F3049-14.

[6]   ASTM F3184 Standard Specification for Additive Manufacturing Stainless Steel Alloy (UNS S31603) with Powder Bed Fusion 1 n.d. doi:10.1520/F3184-16.

[7]   ASTM F3318 Standard for Additive Manufacturing-Finished Part Properties-Specification for AlSi10Mg with Powder Bed Fusion-Laser Beam 1 n.d. doi:10.1520/F3318-18.

[8]   Fitzgerald E, Everhart W. The Effect of Location on the Structure and Mechanical Properties of Selective Laser Melted 316L Stainless Steel. Proc 27th Annu Int Solid Free Fabr Symp 2016:574–83.

[9]   Wang X, Keya T, Chou K. Build Height Effect on the Inconel 718 Parts Fabricated by Selective Laser Melting. Procedia Manuf 2016;5:1006–17. doi:10.1016/j.promfg.2016.08.089.

[10]   Wang Z, Palmer TA, Beese AM. Effect of processing parameters on microstructure and tensile properties of austenitic stainless steel 304L made by directed energy deposition additive manufacturing. Acta Mater 2016;110:226–35. doi:10.1016/j.actamat.2016.03.019.

[11]   Anderson TL. Fracture Mechanics - Fundamentals and Applications. Thrid. 2005. doi:10.1007/978-1-4612-1740-4.

[12]   Ibrahim Y, Li Z, Davies CM, Maharaj C, Dear JP, Hooper PA. Acoustic resonance testing of additive manufactured lattice structures. Addit Manuf 2018;24:566–76. doi:10.1016/j.addma.2018.10.034.

[13]   Karme A, Kallonen A, Matilainen V-P, Piili H, Salminen A. Possibilities of CT Scanning as Analysis Method in Laser Additive Manufacturing. Phys Procedia 2015;78:347–56. doi:10.1016/j.phpro.2015.11.049.

[14]   Jiang R, Kleer R, Piller FT. Predicting the future of additive manufacturing: A Delphi study on economic and societal implications of 3D printing for 2030. Technol Forecast Soc Change 2017;117:84–97. doi:10.1016/j.techfore.2017.01.006.

[15]   Castañón AA& AQ& MAG. Effect of manufacturing parameters on the microstructure and mechanical properties of metal laser sintering parts of precipitate hardenable metals. Int J Adv Manuf Technol 2018.

[16]   Frazier WE. Metal Additive Manufacturing: A Review n.d. doi:10.1007/s11665-014-0958-z.

[17]   Kempen K, Thijs L, Van Humbeeck J, Kruth J-P. Mechanical Properties of AlSi10Mg Produced by Selective Laser Melting. Phys Procedia 2012;39:439–46. doi:10.1016/j.phpro.2012.10.059.

[18]   Zyguła K, Nosek B, Pasiowiec H, Szysiak N. Mechanical properties and microstructure of AlSi10Mg alloy obtained by casting and SLM technique. World Scirntific News n.d.;104:462–72.

[19]   Herzog D, Seyda V, Wycisk E, Emmelmann C. Additive manufacturing of metals. Acta Mater 2016;117:371–92. doi:10.1016/j.actamat.2016.07.019.

[20]   Sames WJ, List FA, Pannala S, Dehoff RR, Babu SS. The metallurgy and processing science of metal additive manufacturing. Int Mater Rev 2016. doi:10.1080/09506608.2015.1116649.

[21]   Olakanmi EO, Cochrane RF, Dalgarno KW. A review on selective laser sintering/melting (SLS/SLM) of aluminium alloy powders: Processing, microstructure, and properties. Prog Mater Sci 2015;74:401–77. doi:10.1016/j.pmatsci.2015.03.002.

[22]   Taheri H, Rashid Bin M, Shoaib M, Koester L, Bigelow T, Collins PC. Powder-based additive manufacturing – a review of types of defects, generation mechanisms, detection, property evaluation and metrology. Int J Addit Subtractive Mater Manuf 2017. doi:10.1504/IJASMM.2017.088204.

[23]   DebRoy T, Wei HL, Zuback JS, Mukherjee T, Elmer JW, Milewski JO, et al. Additive manufacturing of metallic components – Process, structure and properties. Prog Mater Sci 2018;92:112–224. doi:10.1016/j.pmatsci.2017.10.001.

[24]   Maamoun AH, Xue YF, Elbestawi MA, Veldhuis SC. Effect of selective laser melting process parameters on the quality of al alloy parts: Powder characterization, density, surface roughness, and dimensional accuracy. Materials (Basel) 2018;11. doi:10.3390/ma11122343.

[25]   Read N, Wang W, Essa K, Attallah MM. Selective laser melting of AlSi10Mg alloy: Process optimisation and mechanical properties development. Mater Des 2015;65:417–24. doi:10.1016/j.matdes.2014.09.044.

[26]   Aboulkhair NT, Everitt NM, Ashcroft I, Tuck C. Reducing porosity in AlSi10Mg parts processed by selective laser melting. Addit Manuf 2014;1–4:77–86. doi:10.1016/j.addma.2014.08.001.

[27] King WE, Barth HD, Castillo VM, Gallegos GF, Gibbs JW, Hahn DE, et al. Observation of keyhole-mode laser melting in laser powder-bed fusion additive manufacturing. J Mater Process Technol 2014;214:2915–25. doi:10.1016/j.jmatprotec.2014.06.005.

[28] Bourell D, Kruth JP, Leu M, Levy G, Rosen D, Beese AM, et al. Materials for additive manufacturing. CIRP Ann - Manuf Technol 2017;66:659–81. doi:10.1016/j.cirp.2017.05.009.

[29] Saint John D, Joshi S, Simpson T, Qu M, Rowatt J, Lou Y. A Preliminary Examination of Variability Due to Build Location and Powder Feedstock in Additive Manufacture of Inconel 718 using Laser-Based Powder Bed Fusion. Proc 27th Annu Int Solid Free Fabr Symp – An Addit Manuf Conf 2016:542–57.

[30] Johnson KL, Rodgers TM, Underwood OD, Madison JD, Ford KR, Whetten SR, et al. Simulation and experimental comparison of the thermo-mechanical history and 3D microstructure evolution of 304L stainless steel tubes manufactured using LENS. Comput Mech 2018;61:559–74. doi:10.1007/s00466-017-1516-y.

[31] Carroll BE, Palmer TA, Beese AM. Anisotropic tensile behavior of Ti–6Al–4V components fabricated with directed energy deposition additive manufacturing. Acta Mater 2015;87:309–20. doi:10.1016/j.actamat.2014.12.054.

[32] Mugica GW, Tovio DO, Cuyas JC, César González A. Effect of Porosity on the Tensile Properties of Low Ductility Aluminum Alloys. Mater Res 2004;7:221–9.

[33] Hardin RA, Beckermann C. Effect of Porosity on Deformation, Damage, and Fracture of Cast Steel. Metall Mater Trans A 2013;44:5316–5332. doi:10.1007/s11661-013-1669-z.

[34] Direct Metal Laser Sintering [DMLS] Parts On Demand n.d. https://www.stratasysdirect.com/technologies/direct-metal-laser-sintering (accessed October 9, 2019).

[35] ASTM B311 Standard Test Method for Density of Powder Metallurgy (PM) Materials Containing Less Than Two Percent Porosity 1 n.d. doi:10.1520/B0311-17.

[36] EOS GmbH - Electro Optical Systems. EOS Aluminium AlSi10Mg. GPI Prototype Manuf Serv 2014;49:1–5. https://gpiprototype.com/pdf/EOS_Aluminium_AlSi10Mg_en.pdf.

[37] Renishaw. SS 316L-0407 powder for additive manufacturing 2018:1–2. https://resources.renishaw.com/en/details/data-sheet-ss-316l-0407-powder-for-additive-manufacturing--90802.

[38] Yang P, Deibler LA, Bradley DR, Stefan DK, Carroll JD. Microstructure evolution and thermal properties of an additively manufactured, solution treatable AlSi10Mg

part. J Mater Res 2018. doi:10.1557/jmr.2018.405.

[39]   Finfrock CB, Exil A, Carroll JD, Deibler L. Effect of Hot Isostatic Pressing and Powder Feedstock on Porosity, Microstructure, and Mechanical Properties of Selective Laser Melted AlSi10Mg. Metallogr Microstruct Anal 2018;7:443–56. doi:10.1007/s13632-018-0456-z.

[40]   Zakay A, Aghion E. Effect of Post-heat Treatment on the Corrosion Behavior of AlSi10Mg Alloy Produced by Additive Manufacturing. J Miner Met Mater Soc n.d. doi:10.1007/s11837-018-3298-x.

[41]   Brandl E, Heckenberger U, Holzinger V, Buchbinder D. Additive manufactured AlSi10Mg samples using Selective Laser Melting (SLM): Microstructure, high cycle fatigue, and fracture behavior. Mater Des 2012;34:159–69. doi:10.1016/j.matdes.2011.07.067.

[42]   Li W, Li S, Liu J, Zhang A, Zhou Y, Wei Q, et al. Effect of heat treatment on AlSi10Mg alloy fabricated by selective laser melting: Microstructure evolution, mechanical properties and fracture mechanism. Mater Sci Eng A 2016;663:116–25. doi:10.1016/j.msea.2016.03.088.

[43]   Uzan NE, Shneck R, Yeheskel O, Frage N. Fatigue of AlSi10Mg specimens fabricated by additive manufacturing selective laser melting (AM-SLM). Mater Sci Eng A 2017;704:229–37. doi:10.1016/j.msea.2017.08.027.

[44]   Yang P, Rodriguez MA, Deibler LA, Jared BH, Griego J, Kilgo A, et al. Effect of thermal annealing on microstructure evolution and mechanical behavior of an additive manufactured AlSi10Mg part 2019. doi:10.1557/jmr.2018.82.

[45]   Han Q, Jiao Y. Effect of heat treatment and laser surface remelting on AlSi10Mg alloy fabricated by selective laser melting n.d. doi:10.1007/s00170-018-03272-y.

[46]   Zhuo L, Wang Z, Zhang H, Yin E, Wang Y, Xu T, et al. Effect of post-process heat treatment on microstructure and properties of selective laser melted AlSi10Mg alloy. Mater Lett 2019;234:196–200. doi:10.1016/j.matlet.2018.09.109.

[47]   ASTM. ASTM E399 Standard Test Method for Linear-Elastic Plane-Strain Fracture Toughness KIc of Metallic Materials1 2019:1–34. doi:10.1520/E0399-09E02.2.

[48]   ASTM. Standard Test Methods of Compression Testing of Metallic Materials at Room Temperature n.d. https://compass.astm.org/download/E9.30253.pdf (accessed September 25, 2019).

[49]   Bartanus JB. An Experimental Study of Geometric Defects and Their Significance on Material Properties and Behavior. Clemson University, 2018.

[50]   Gong H, Rafi K, Gu H, Starr T, Stucker B. Analysis of defect generation in Ti–6Al–4V parts made using powder bed fusion additive manufacturing processes.

Addit Manuf 2014;1–4:87–98. doi:10.1016/j.addma.2014.08.002.

[51]   Zhang B, Li Y, Bai Q. Defect Formation Mechanisms in Selective Laser Melting: A Review. Chinese J Mech Eng (English Ed 2017;30:515–27. doi:10.1007/s10033-017-0121-5.

[52]   Murakami, Y., Aoki, S. Hasebe, N. Itoh, Y., Miyata, H., Miyazaki, N., Terada, H. Tohgo, K., Toya , M., Yuuki R. Stress Intensity Factors Handbook Vol 1. 1990.

[53]   William D. Callister J, David G. Rethwisch. Material Science And Engineering An Introduction. 2009. doi:doi:10.4324/9780203478981.ch3.

[54]   Wilson-Heid AE, Novak TC, Beese AM. Characterization of the Effects of Internal Pores on Tensile Properties of Additively Manufactured Austenitic Stainless Steel 316L. Exp Mech 2019:793–804. doi:10.1007/s11340-018-00465-0.

[55]   Yegyan Kumar A, Wang J, Bai Y, Huxtable ST, Williams CB. Impacts of process-induced porosity on material properties of copper made by binder jetting additive manufacturing. Mater Des 2019;182:108001. doi:10.1016/j.matdes.2019.108001.

[56]   Drahansky M, Paridah M., Moradbak A, Mohamed A., Owolabi F abdulwahab taiwo, Asniza M, et al. Fracture Toughness of Metal Castings. Sci. Technol. Cast. Process. Fig., 2016, p. 285–312. doi:http://dx.doi.org/10.5772/57353.

[57]   Hall EO. The deformation and ageing of mild steel: II Characteristics of the Lüders deformation. Proc Phys Soc Sect B 1951;64:742–7. doi:10.1088/0370-1301/64/9/302.